Simulation of Corneal imaging properties for near objects

Journal Item

Received: 19 April 2021 | Accepted: 17 June 2021

DOI: 10.1111/opo.12861

OPO THE COLLEGE OF OPTOMETRISTS

ORIGINAL ARTICLE

Simulation of Corneal imaging properties for near objects

Achim Langenbucher[1] | **Timo Eppig**[1] | **Alan Cayless**[2] | **Zisis Gatzioufas**[3] | **Jascha Wendelstein**[4] | **Peter Hoffmann**[5] | **Nóra Szentmáry**[6,7]

[1]Department of Experimental Ophthalmology, Saarland University, Homburg/Saar, Germany

[2]School of Physical Sciences, The Open University, Milton Keynes, UK

[3]Department of Ophthalmology, University Hospital Basel, Basel, Switzerland

[4]Department of Ophthalmology, Johannes Kepler University Linz, Linz, Austria

[5]Augen- und Laserklinik Castrop-Rauxel, Castrop-Rauxel, Germany

[6]Dr Rolf M Schwiete Center for Limbal Stem Cell and Aniridia Research, Saarland University, Homburg/Saar, Germany

[7]Department of Ophthalmology, Semmelweis-University, Budapest, Hungary

Correspondence
Achim Langenbucher, Department of Experimental Ophthalmology, Saarland University, Homburg/Saar, Germany.
Email: achim.langenbucher@uks.eu

Abstract

Purpose: Using raytracing simulation to study the effect of corneal imaging metrics for different aperture sizes as a function of object distances with different schematic model eyes.

Methods: This raytracing simulation determined the best focus (with the least root-mean-square (rms) ray scatter) and the best wavefront focus (with least rms wavefront error) for four schematic model eyes (Liou-Brennan (LBME), Atchison (ATCHME), Gullstrand (GULLME) and Navarro (NAVME)) with 4 aperture sizes (2–5 mm) and 30 object distances in a logscale from 10 cm to 10 m plus infinity. For each configuration, 10,000 rays were traced through the cornea, and the aperture stop was located at the lens front apex plane as described in the model eyes. The wavefront was decomposed into Zernike components to extract the spherical aberration term.

Results: The focal distance with respect to the corneal front apex increases from around 31 mm for objects at infinity to around 40 mm for objects at 10 cm. The best (wavefront) focus was systematically closer to the cornea compared with the paraxial focus, and the overestimation of focal length with the paraxial focus was larger for large aperture sizes and small object distances. The rms ray scatter and wavefront error were both systematically larger with large aperture and small object sizes. At best focus the rms wavefront error was systematically larger, and the rms ray scatter was systematically smaller compared to the best wavefront focus. Spherical aberration varied more with GULLME than with LBME or NAVME, and increased strongly at smaller object distances.

Conclusions: The imaging properties of the cornea, especially spherical aberration, increase strongly as the object distance decreases. This effect should be considered, especially when considering aberration correcting lenses for near vision such as multifocal or enhanced depth of focus lenses.

KEYWORDS
best focus, corneal imaging properties, near vision, spherical aberration model eye, wavefront aberration

INTRODUCTION

In recent decades, a range of new intraocular lens (IOL) designs have been proposed. In addition to classical lenses with a spherical optic design on each side, aspheric lenses that address the spherical aberration of the cornea have been introduced. Some of these, with low negative asphericity on one or both optical surfaces, aim to correct the intrinsic spherical aberrations of the IOL (so-called aberration-free IOL) when positioned in a collimated or a convergent light beam; others, with a larger amount of negative asphericity (so-called aberration correcting IOL), aim for negative spherical aberration in the lens, in order to correct for the positive spherical aberration of the cornea.

Multifocal lenses, which promise spectacle independence by simultaneously generating images from objects positioned at varying distances from the retina, have also been launched.[1] Different design concepts have been proposed, such as refractive or diffractive designs, or maintaining 2 (bifocal), 3 (trifocal) or more distinct foci. Some have a high near addition for reading (multifocal IOL) or a low addition for maintaining both far and intermediate distance vision (Enhanced depth of focus, EDOF). Multifocal and EDOF lens designs typically correct some degree of spherical aberration, either the intrinsic spherical aberration of the IOL or even the spherical aberration of the cornea.[1]

However, given that such multifocal or EDOF lens designs are used to maintain intermediate or near vision, the corneal aberrations when imaging objects at near distances must be considered.[2,3] For example, a cornea based on the Liou-Brennan schematic model eye[4] shows around 0.26 µm of spherical aberration over a 6 mm central zone. With other model eyes, such as the Gullstrand schematic eye[5] with spherical surfaces, the spherical aberration is even higher.[6,7] But for objects at near distances this magnitude cannot be assumed to remain constant. When viewing near objects, optical aberrations change with viewing distance, and especially with multifocal lenses designed to image both far and near objects. This is also true for EDOF designs used for far and intermediate vision; here, the optical aberrations of the cornea when imaging far and near or far and intermediate objects must be considered.[3]

The purpose of this simulation study was to analyse the imaging properties of the cornea using several schematic model eyes, including the Liou-Brennan, Atchison, Gullstrand and Navarro. The terms of the analysis are best focus and best wavefront position, and to derive the change in root-mean-squared (rms) spot size, rms wavefront error and spherical aberration with various pupil sizes while imaging objects from infinity to intermediate and near distances using raytracing strategies.

Key points

- Since aberrations change with object distance, simulations and raytracing investigating ocular imaging performance should consider near objects with a retinal imaging plane, rather than distant objects and a shifted plane.
- Paraxial calculations systematically overestimate the focal distance for model eyes, and root-mean-squared ray scatter and wavefront error are systematically increased for large pupil sizes and near objects.
- Corneal spherical aberration of model eyes in a 6 mm zone increases slightly with aperture size, and also increases systematically for objects at near distances.

METHODS

For this simulation study, a raytracing setup was implemented for the anterior segment of four different schematic model eyes: The Liou Brennan model eye (LBME[4]), the Atchison model eye (ATCHME[8,9]), the Gullstrand model eye (GULLME[5]) and the Navarro model eye (NAVME[10,11]). The anterior segment specifications of the model eyes tested are listed in *Table 1*.

The LBME is characterised by four coaxial refracting surfaces, an aperture stop located at the lens front surface which is nasally displaced by 0.5 mm, and an incident beam tilted 5° nasally to account for the eccentric location of the fovea. Both corneal surfaces are considered aspherical.[4]

The ATCHME, the GULLME and the NAVME are all designed with coaxial optical elements and a coaxial incident beam. The cornea of the ATCHME has an aspherical front and back surface,[8] whereas the cornea of the NAVME has an aspherical front surface and spherical back surface.[11] The cornea of the GULLME is characterised by spherical front and back surfaces.[5]

The aperture stop was located at the front lens plane of each model eye. Aperture size varied from 2 to 5 mm in 1 mm steps, which equates to a visible (entrance) pupil size from around 2.4 to 6.0 mm. For each model eye and aperture stop diameter, 10,000 rays were initialised from a point light source (divergent ray bundle with an equally-spaced grid distribution of 7 mm at the corneal front apex plane), with object distances varying from 10 cm to 10 m in a uniform logarithmic scale, and a collimated beam starting from a plane 1 cm in front of the cornea with equally spaced parallel rays within a circular pupil of 7 mm. In total, $4 \times 4 \times 31$ scenarios were considered.

Raytracing was implemented in MATLAB version 2019b (MathWorks, mathworks.com). For each scenario (i.e., model eye, aperture size and object distance) the best focus was determined in terms of minimising the rms ray scatter at the focal plane.[12] In addition, the best wavefront focus was calculated in terms of rms variation of the optical path length from the object (a point source for objects at finite distances or a plane for the

TABLE 1 Specifications of the four schematic model eyes under test: R_a/R_p refer to the central corneal front and back surface curvature, Q_a/Q_p to the corneal front and back surface asphericity, d_C to the central corneal thickness, n_C and n_A to the refractive index of cornea and aqueous humour

Model eye	R_a in mm	Q_a	R_p in mm	Q_p	d_C in mm	Aperture size (axial/ateral) in mm	n_C	n_A	Angle of the incident beam
Liou-Brennan	7.77	−0.18	6.40	−0.60	0.50	3.16/0.5 mm nasally	1.3376	1.336	5° from nasally
Atchison	7.77	−0.15	6.40	−0.275	0.55	3.15/centred	1.376	1.3374	Coaxial
Gullstrand	7.70	0.00	6.80	0.00	0.50	3.10/centred	1.376	1.336	Coaxial
Navarro	7.72	−0.26	6.50	0.00	0.55	3.00/centred	1.376	1.3374	Coaxial

The axial position of the aperture stop is provided as the distance from the corneal back surface apex. The Liou-Brennan model eye considers a decentred aperture stop and a tilted incident beam; all other model eyes are strictly centred and coaxial.

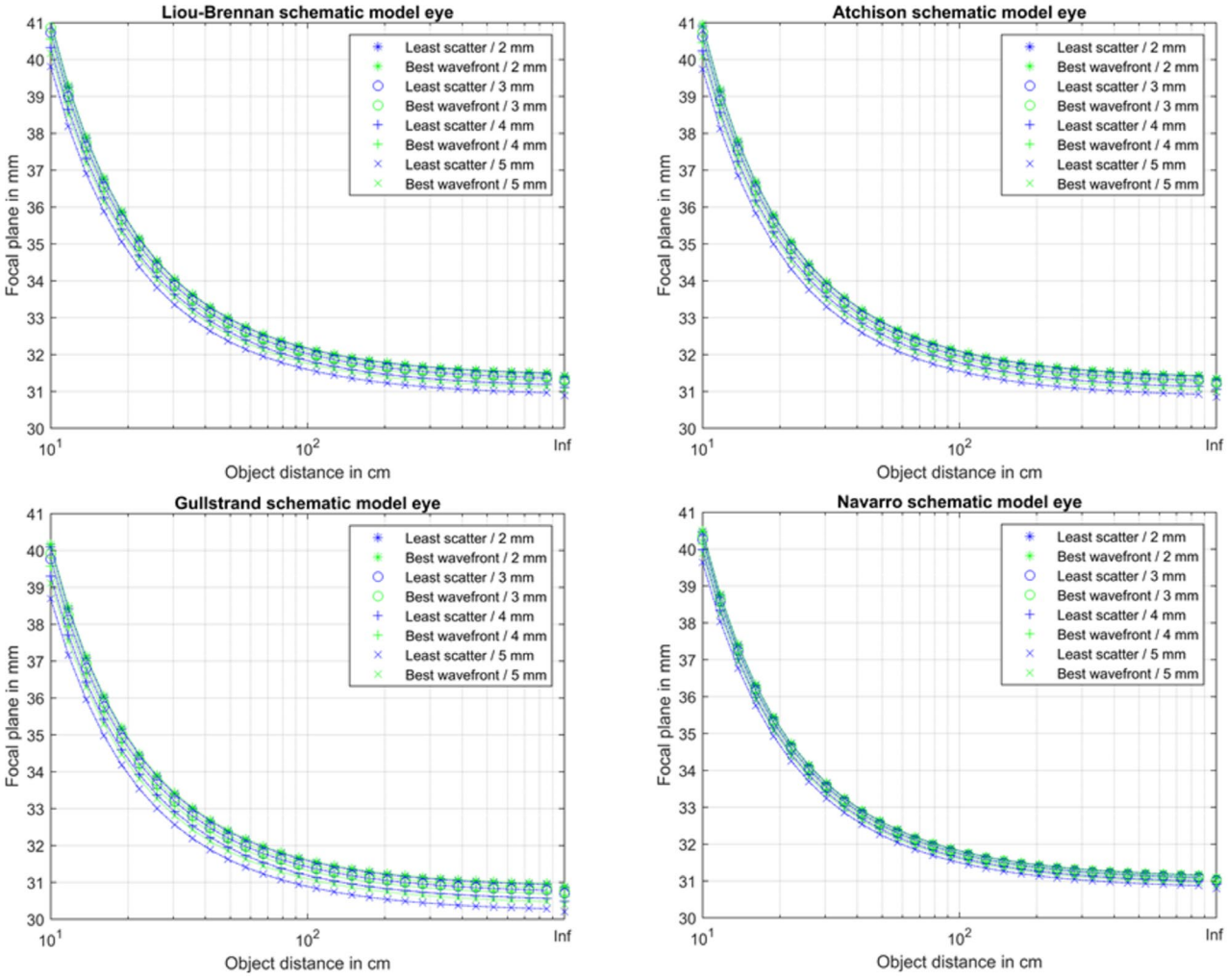

FIGURE 1 Position of the best focus plane (blue) and best wavefront focus plane (green) for the model cornea and aperture sizes 2–5 mm as a function of object distance varied from 10 cm to 10 m and for infinity (Inf). a (upper left), b (upper right), c (lower left), and d (lower right) shows the situation for the cornea of the Liou-Brennan/Atchison/Gullstrand/Navarro schematic model eyes, respectively

collimated beam) to the focal point. The location of best focus and best wavefront focus was determined based on a nonlinear search algorithm[13,14] for each schematic model eye for aperture sizes from 2 to 5 mm (in 1 mm steps) as a function of object distance. In addition to the location of the best focus and best wavefront focus, we analysed the rms ray scatter and the spherical aberration term Z_4^0 from a Zernike decomposition of the wavefront referenced to a 6mm circle considered at the corneal front surface plane. All simulations were performed in a monochromatic fashion using the nominal refractive indices listed in *Table 1*.

RESULTS

For a collimated incident beam from an object at infinity, the location of the best focus with respect to the corneal front apex plane for the LBME/ATCHME/GULLME/NAVME for a 3 mm aperture was 31.2790 (temporal: 2.0443 mm)/31.2170 mm/30.7041 mm/31.0091 mm. The location of the best wavefront focus was 31.3348 mm (temporal: 2.0 495 mm)/31.2694 mm/30.7734 mm/31.0395 mm, respectively. The axial location of the best focus (in blue) and best wavefront focus (in green) for object distances from 10 cm to 10 m, and for a collimated beam (object at infinity) and 2–5 mm aperture sizes are shown in *Figure 1* (1a: LBME, 1b: ATCHME, 1c: GULLME, 1d: NAVME). The focus moved from approximately 31 mm for objects at infinity to around 40 mm for objects at 10 cm for all model eyes and aperture sizes.

Figure 2 shows the axial position of the best focus (in blue) and the best wavefront focus (in green) for the four model eyes (2a: LBME, 2b: ATCHME, 2c: GULLME, 2d: NAVME) with respect to the paraxial focus calculated using classical vergence formulae for 2–5 mm aperture sizes and object distances from 10 cm to 10 m. As a result of the positive spherical aberration of the cornea with all schematic model eyes, this focal length is systematically shorter than the focal length from the paraxial calculations. For large pupil sizes and near objects, the deviation of the best focus and best wavefront focus from the paraxial focus is more pronounced compared with small aperture sizes and distant objects. As an example, for a 3 mm aperture, the best focus/best wavefront focus is 0.2855/0.2296 mm, 0.2095/0.1571 mm, 0.2767/0.2074 mm and 0.1218/0.0914 mm closer to the cornea compared with the paraxial focus for distant objects using the LBME, ATCHME, GULLME and NAVME models, respectively. For objects at 10 cm, the respective best focus/best wavefront focus is even further from the paraxial focus and closer to the cornea (0.7083/0.5741 mm, 0.5051/0.3789 mm, 0.6090/0.4566 mm and 0.3611/0.2711 mm).

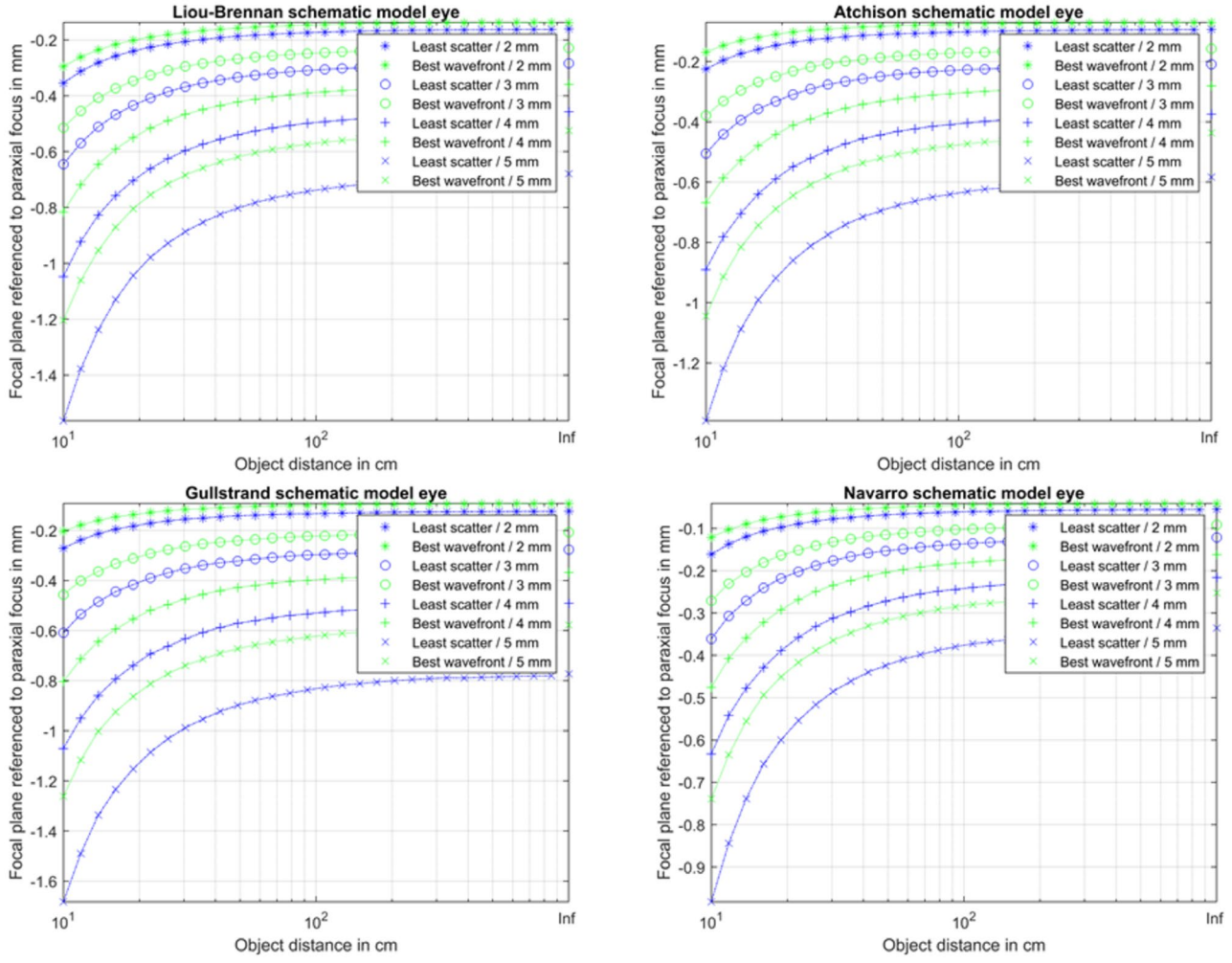

FIGURE 2 Position of the best focus plane (blue) and best wavefront focus plane (green) with respect to the paraxial focus derived from a vergence calculation for the model cornea and aperture sizes 2–5 mm as a function of object distance varied from 10 cm to 10 m and for infinity (Inf). a (upper left), b (upper right), c (lower left), and d (lower right) shows the situation for the cornea of the Liou-Brennan/Atchison/Gullstrand/Navarro schematic model eyes, respectively

In *Figure 3*, the rms ray scatter at the focal plane is plotted for all four schematic model eyes (3a: LBME, 3b: ATCHME, 3c: GULLME, 3d: NAVME), for 2–5 mm aperture sizes as a function of object distance. The ray scatter at the best focus plane is depicted in blue, and for the best wavefront focal plane in green. In general, ray scatter increases with the size of the aperture stop and decreases with object distance. As a consequence of the best focus being determined from an optimisation for the least ray scatter, the ray scatter is systematically smaller compared with that at the best wavefront focus plane. As an example, for a 3 mm aperture, the rms ray scatter at the best focus plane/best wavefront focus plane is 3.0876/3.7596 µm, 2.8425/3.4828 µm, 3.8170/4.6794 µm and 1.6558/2.0275 µm for distant objects with the LBME, ATCHME, GULLME and NAVME models. For objects at 10 cm, the respective ray scatter at best focus/best wavefront focus plane is systematically larger, namely 10.4469/11.1282 µm, 5.0971/6.2558 µm, 6.2743/7.7059 µm and 3.6778/4.5097 µm, respectively.

Figure 4 shows the rms wavefront error at the focal plane for all four schematic model eyes (4a: LBME, 4b: ATCHME, 4c: GULLME, 4d: NAVME) for 2–5 mm aperture sizes as a function of object distance from 10 cm to 10 m, respectively. The rms wavefront error at the best focus plane is depicted in blue, and the best wavefront focal plane in green. As a consequence of the best wavefront focus being determined by minimising the wavefront error, the rms wavefront error is systematically smaller compared with the wavefront error at the best focus plane. As an example, for a 3 mm aperture, the rms wavefront error at the best focus plane/best wavefront focus plane is 0.0416/0.0271 µm, 0.0377/0.0231 µm, 0.0515/0.0314 µm and 0.0220/0.0135 µm for distant objects with the LBME, ATCHME, GULLME and NAVME models, respectively. For objects at 10 cm, the respective wavefront error at best focus/best wavefront focus plane is systematically larger at 0.1335/0.1264 µm, 0.0507/0.0309 µm, 0.0638/0.0388 µm and 0.0369/0.0226 µm.

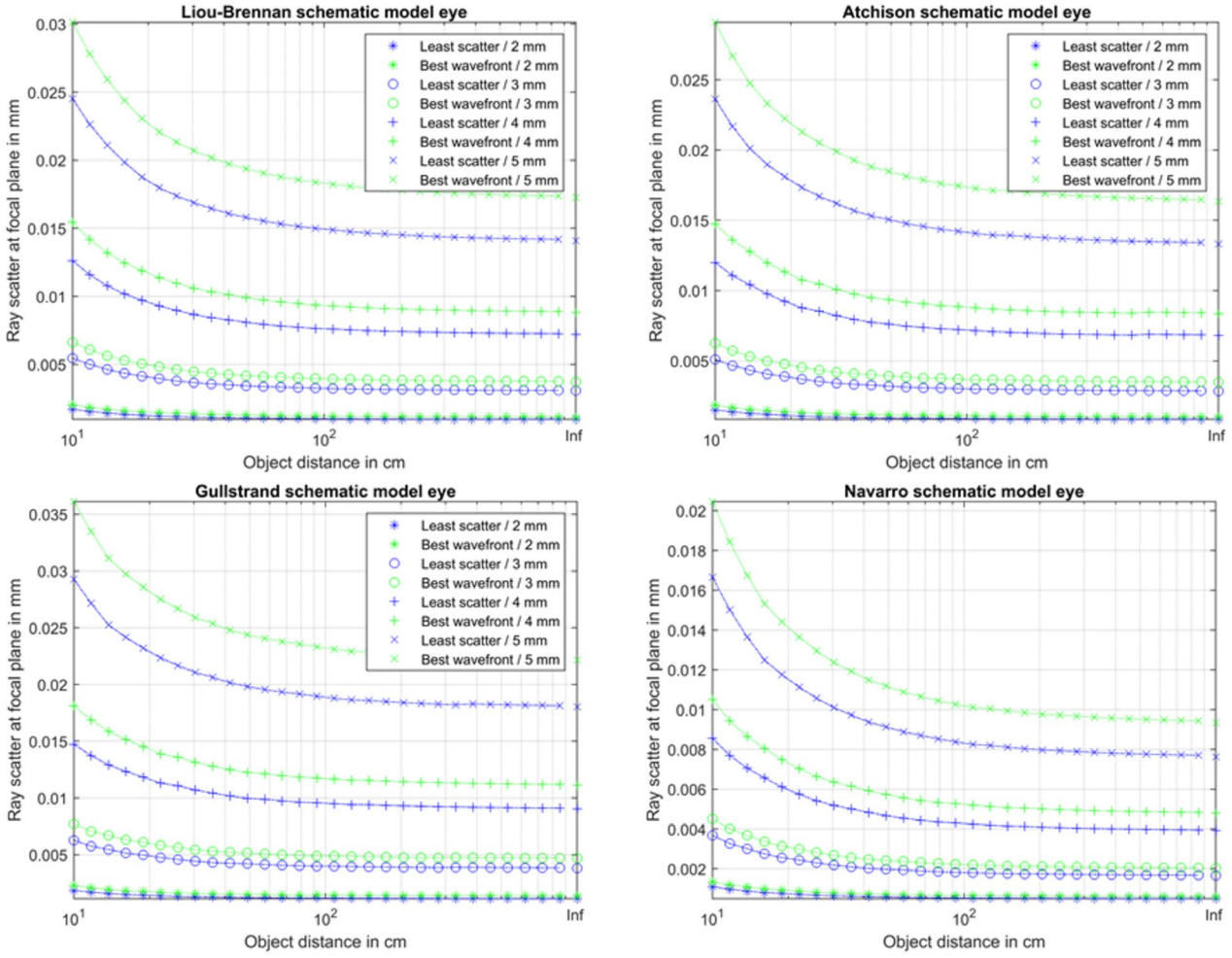

FIGURE 3 Root-mean-squared (rms) ray scatter at best focus plane (blue) and at best wavefront focus plane (green) for the model cornea and aperture sizes 2–5 mm as a function of object distance varied from 10 cm to 10 m and for infinity (Inf). a (upper left), b (upper right), c (lower left), and d (lower right) shows the situation for the cornea of the Liou-Brennan/Atchison/Gullstrand/Navarro schematic model eyes, respectively

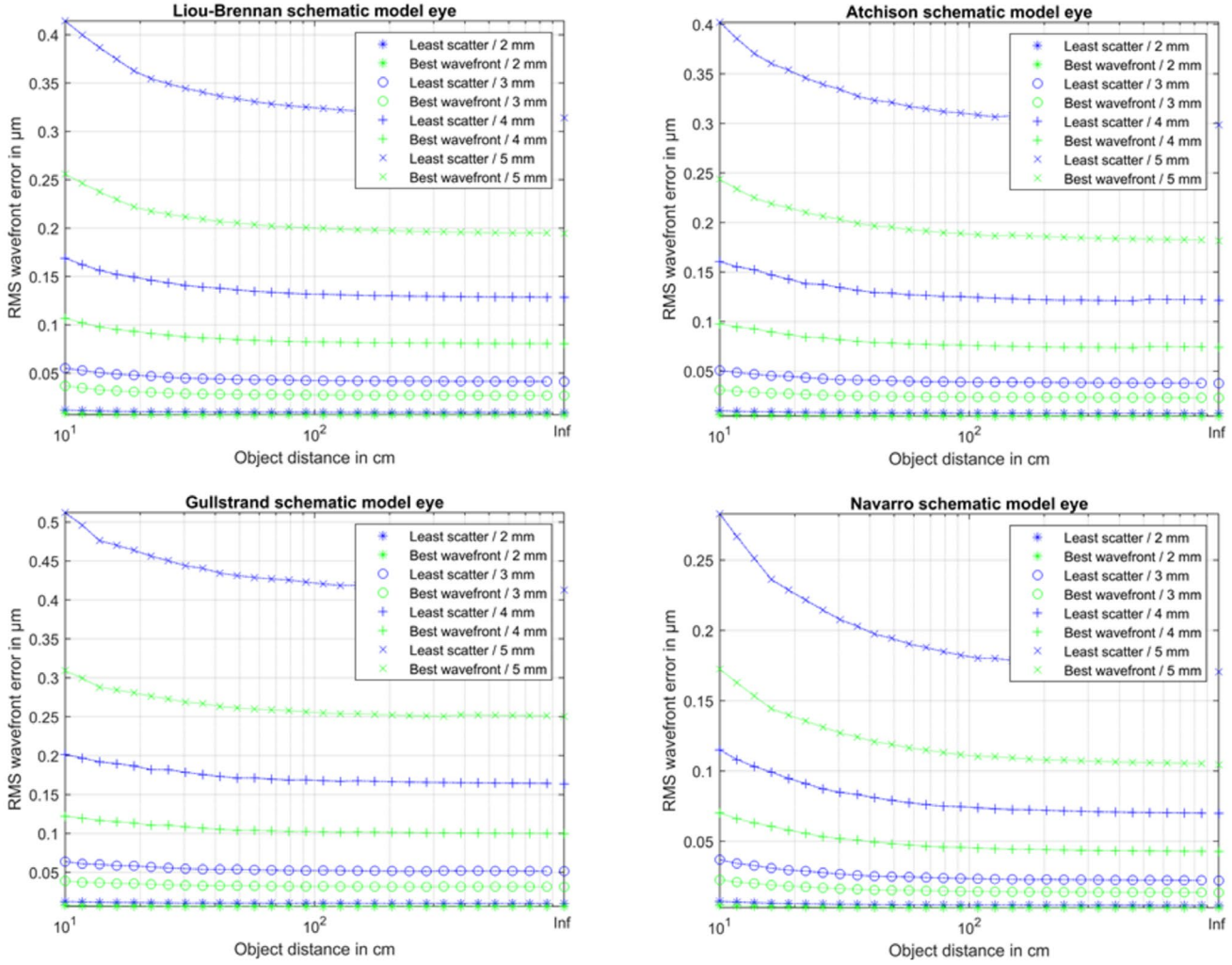

FIGURE 4 Root-mean-squared (rms) wavefront error at best focus plane (blue) and at best wavefront focus plane (green) for the model cornea and aperture sizes 2–5 mm as a function of object distance varied from 10 cm to 10 m and for infinity (Inf). a (upper left), b (upper right), c (lower left), and d (lower right) shows the situation for the cornea of the Liou-Brennan/Atchison/Gullstrand/Navarro schematic model eyes, respectively

The spherical aberration term Z_4^0 extracted from the wavefront error within a reference circle of 6 mm at the corneal front surface plane is shown in *Figure 5* for all four schematic model eyes (5a: LBME, 5b: ATCHME, 5c: GULLME, 5d: NAVME) and for 2–5 mm aperture sizes as a function of object distance from 10 cm to 10 m, respectively. With increasing aperture size and smaller object distances, the spherical aberration term increases systematically. The spherical aberration term for the best focus plane/the best wavefront focus plane is depicted in blue/green. As the Gullstrand schematic model eye uses spherical surfaces for the cornea, this model yields the highest values of corneal spherical aberration, whereas the Navarro schematic model eye yields the lowest corneal spherical aberration. As an example, for a 3 mm aperture, the spherical aberration (referenced to a 6 mm zone corneal front surface) for best focus plane/best wavefront focus plane is 0.2732/0.2741 µm, 0.2539/0.2547 µm, 0.3461/0.3472 µm and 0.1506/0.1511 µm for distant objects with the LBME, ATCHME, GULLME and NAVME models, respectively. For objects at 10 cm, the respective spherical aberration for best focus/best wavefront focus plane is systematically larger at 0.4016/0.4025 µm, 0.3768/0.3777 µm, 0.4730/0.4741 µm and 0.2748/0.2755 µm.

DISCUSSION

There is much discussion regarding the imaging performance of IOLs, especially in an era of aspheric, aberration free and aberration correcting lens designs, with multifocal and enhanced depth of focus lenses.[1] Most of the controversial discussions on aspheric lenses concern the amount of spherical aberration that should be corrected for comfortable vision; some researchers postulate that corneal spherical aberration should be fully corrected, while others propose a moderate correction of corneal aberration to maintain the robustness of the lens to

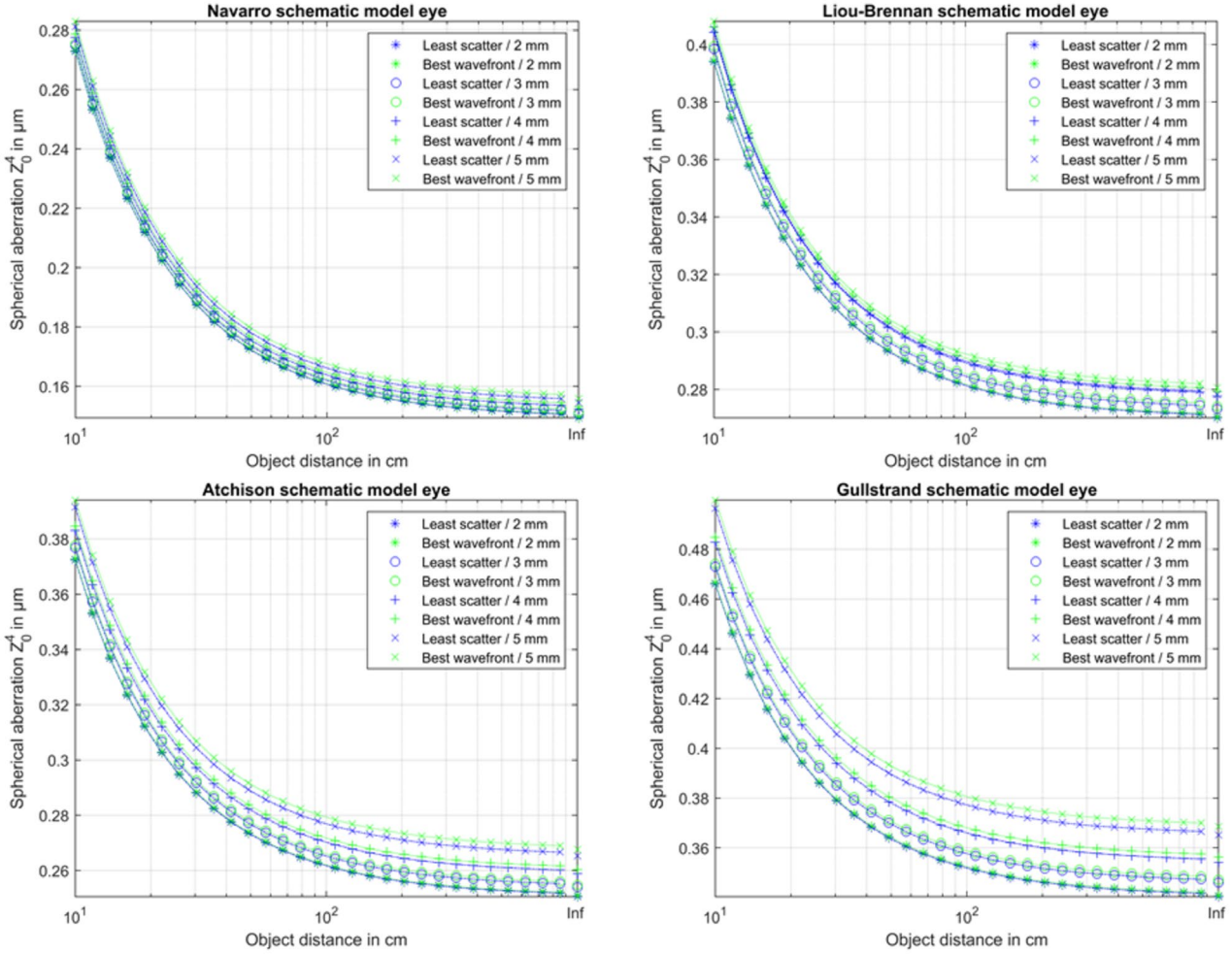

FIGURE 5 Spherical aberration term Z40 extracted from the wavefront error referenced to a circle with diameter of 6 mm. Spherical aberration is determined for the best focus plane (blue) and the best wavefront focus plane (green) for the model cornea and aperture sizes 2–5 mm as a function of object distance varied from 10 cm to 10 m and for infinity (Inf). a (upper left), b (upper right), c (lower left), and d (lower right) shows the situation for the cornea of the Liou-Brennan/Atchison/Gullstrand/Navarro schematic model eyes, respectively

displacement and tilt. However, after cataract surgery, the resulting (spherical) aberration of the pseudophakic eye results from corneal aberration, lens aberration and the alignment of the cornea and lens relative to the visual axis and the outline of the pupil. Schematic model eyes reflect an average behaviour of ocular imaging, and the description of the cornea varies across model eyes.[7] For example, with the GULLME all surfaces are spherical and coaxial.[5,15] In other schematic model eyes such as the ATCHME or the NAVME eyes, the surfaces are aligned but have, at least in part, an aspherical shape.[8,6,11] In the LBME, the surfaces are aspherical, the lens shows a gradient index structure, the aperture stop is defined explicitly and the incident ray is slanted towards the axis of symmetry of the refracting surfaces in order to account for the eccentric position of the fovea in the human eye.[4] As a consequence, the aperture stop is shifted by 0.5 mm in the nasal direction so that an incident ray bundle passes through the aperture stop and is focused on the fovea.

However, multifocal and EDOF lenses are designed to maintain 'pseudoaccommodation'. There are different options to achieve multifocality, either with diffractive structures or with refractive designs which are rotationally symmetric or use sectors or zones to allow near vision.[1] When considering lenses which are designed for simultaneously imaging both far and near objects onto the retina, the imaging properties of the cornea for both far and near distance objects have to be considered. However, most studies focus on the imaging properties of the cornea for distant objects, and ignore the change in imaging behaviour when viewing near objects.

In the present investigation we analysed imaging properties of the corneas of four schematic model eyes in a simulation setup for 2–5 mm apertures as a function of the object distance. This simulation was performed with numerical raytracing using the curvature, asphericity and refractive index data of the LBME, ATCHME, GULLME, and NAVME as shown in *Table 1*. For the LBME

we considered the incident ray to be slanted by 5° towards the axis of symmetry as defined by the refracting surfaces, and the aperture stop to be decentred 0.5 mm nasally. The ATCHME, GULLME, and NAVME are all strictly coaxial and centred. For simulation of distant objects we defined a collimated beam with a diameter of 7 mm, and for the simulation of near objects we used a point light source located at the respective object distance, with a divergent beam having an equidistant ray pattern and a diameter of 7 mm at the corneal front apex plane. The rays were followed through the cornea with the aperture stop located at the front lens apex plane. There is no unique definition of best focus, and the choice of which plane is defined as best focus will depend on the application. In this study we used two different measures for best focus; the best focus plane was defined as the focus with the least rms scatter,[12] and the best wavefront focus plane was defined as the plane with the least rms wavefront error. For each schematic model eye and aperture size, we defined the location of the best focus and the best wavefront focus for 30 object distances in a logscale from 10 cm to 10 m plus infinity, and analysed the ray scatter together with the wavefront error in terms of optical path length differences from the source to the image.

The best focus and the best wavefront focus are located coaxially for the ATCHME, the GULLME and the NAVME, but off-axis for the LBME. The axial distance with respect to the anterior corneal apex increased from around 31 mm for objects at infinity to approximately 40 mm for objects positioned 10 cm in front of the eye for aperture sizes of 2 – 5 mm (*Figure 1*). Comparing the best focus and best wavefront focus position with the respective paraxial focus derived from vergence calculations, we find that as a consequence of spherical aberration, both best focus positions are systematically closer to the cornea, and the offset increases with aperture size and decreases with object distance as shown in *Figure 2*. It is not surprising that the ray scatter increases systematically with aperture size as shown in *Figure 3*, but it also decreases with object distance. In addition, we find that the ray scatter is systematically larger with the best wavefront focus compared to the best focus plane, meaning that the target criterion for searching the focus position has a large impact on the ray scatter properties. It is also not surprising that for a larger aperture size the rms wavefront error increases for all four model eyes as shown in *Figure 4*. The wavefront error also decreases systematically with the object distance, and is systematically larger at best focus compared to best wavefront focus, which again supports the conclusion that the target criterion for searching the focus position affects the imaging metrics.

The most interesting finding of this study is that the spherical aberration term Z_4^0 of the Zernike decomposition of wavefront error referenced to a 6 mm zone (often used for selecting the appropriate aspherical lens design) shows a large decrease with object distance. For instance, in the LBME, the spherical aberration which is known to be around 0.26 µm (depending on the aperture size) for objects located at infinity, increases to 0.4 µm or more for object distances of 10 cm. With the GULLME with spherical surfaces, this increases from around 0.36 µm for objects at infinity to values of around 0.46–0.50 µm for objects at 10 cm. For corneas of model eyes with larger spherical aberration (e.g., the GULLME with spherical surfaces), the effect of aperture size is much more pronounced compared with corneas of model eyes having low spherical aberration (e.g., the NAVME or LBME).

As a clinical consequence, especially for multifocal and EDOF lenses, even a so-called fully-correcting lens design intended to compensate for the total spherical aberration of an average cornea (e.g., the LBME) for distant objects will not correct the spherical aberration for near vision; this lens design will only partly correct spherical aberration at near. This image deterioration due to the residual (uncorrected) spherical aberration for near objects must be taken into account.

In conclusion, the imaging characteristics of the cornea for near objects are frequently ignored. Using a ray-tracing simulation study on the Liou-Brennan, Atchison, Gullstrand and Navarro schematic model eyes, we found that:

1. the focal distance of the cornea increases significantly with a decrease in object distance from around 31 mm for objects at infinity to approximately 40 mm for objects at 10 cm;
2. paraxial calculation systematically overestimates the focal distance, especially for larger aperture sizes and smaller object distances;
3. rms ray scatter at the focal plane is systematically increased with larger aperture sizes and shorter object distances;
4. rms wavefront error is systematically increased with larger aperture sizes and shorter object distances;
5. the spherical aberration term of the wavefront error is slightly increased for larger aperture sizes (depending on the model eye) and systematically greater for small object distances and
6. rms ray scatter and wavefront error differ significantly if the focus is defined as best focus (least rms ray scatter at the focal plane) or best wavefront focus (least rms wavefront error with respect to the central 6 mm zone at the corneal front surface). This means that the optimisation of focus on ray scatter is strictly at the cost of wavefront error and vice versa.

ACKNOWLEDGEMENT

This work was supported in part by the Dr Rolf M Schwiete Foundation, Mannheim, Germany

CONFLICT OF INTEREST

The authors report no conflicts of interest and have no proprietary interest in any of the materials mentioned in this article.

AUTHOR CONTRIBUTION

Achim Langenbucher: Conceptualization (equal); Investigation (equal); Methodology (equal); Resources (equal); Software (equal); Validation (equal); Writing-original draft (equal). **Timo Eppig:** Formal analysis (equal); Validation (equal). **Alan Cayless:** Project administration (equal); Supervision (equal); Writing-original draft (equal). **Zisis Gatzioufas:** Data curation (equal); Project administration (equal); Validation (equal). **Jascha Wendelstein:** Data curation (equal); Resources (equal). **Peter Hoffmann:** Methodology (equal); Visualization (equal). **Nóra Szentmáry:** Conceptualization (equal); Investigation (equal); Project administration (equal); Supervision (equal); Writing-original draft (equal).

ORCID

Achim Langenbucher https://orcid.org/0000-0001-9175-6177

REFERENCES

1. Rampat R, Gatinel D. Multifocal and extended depth-of-focus intraocular lenses in 2020. *Ophthalmology*. 2020. S0161-6420(20)30931-3. https://doi.org/10.1016/j.ophtha.2020.09.026. Epub ahead of print.
2. Fritzsch M, Dawczynski J, Jurkutat S, Vollandt R, Strobel J. Aberrationen höherer Ordnung bei Akkommodation. Dynamische Wellenfrontmessung [Monochromatic aberration in accommodation. Dynamic wavefront analysis]. *Ophthalmologe* 2011;108:553–560. https://doi.org/10.1007/s00347-011-2336-7. Erratum in: Ophthalmologe. 2011 108(10):979. Jurkutat, S [added]. PMID: 21695608.
3. Shetty N, Kochar S, Paritekar P, Artal P, Shetty R, Nuijts RMMA, et al. Patient-specific determination of change in ocular spherical aberration to improve near and intermediate visual acuity of presbyopic eyes. *J Biophotonics*. 2019;12:e201800259. https://doi.org/10.1002/jbio.201800259
4. Liou HL, Brennan NA. Anatomically accurate, finite model eye for optical modeling. *J Opt Soc Am A*. 1997;14:1684–1695.
5. Gullstrand A. Anhang zu Teil 1. In: von Helmholtz H, editor. Physiologische Optik, 3rd ed., vol. 1. Hamburg: Voss; 1909. pp. 350–358.
6. Rabbetts RB. In Bennett & Rabbetts' Clinical visual optics. 4th ed. Edinburgh: Butterworth – Heinemann – Elsevier; 2007.
7. Gross H, Blechinger F, Achtner B. The human eye. In: Handbook of optical systems, chapter 36, Weinheim: Wiley; 2008.
8. Atchison DA, Thibos LN. Optical models of the human eye. *Clin Exp Optom*. 2016;99:99–106.
9. Atchison DA. Age-related paraxial schematic emmetropic eyes. *Ophthalmic Physiol Opt*. 2009;29:58–64.
10. Navarro R, Rozema JJ, Tassignon MJ. Optical changes of the human cornea as a function of age. *Optom Vis Sci*. 2013;90:587–598.
11. Navarro R, Santamaría J, Bescós J. Accommodation-dependent model of the human eye with aspherics. *J Opt Soc Am A*. 1985;2:1273–1281.
12. Langenbucher A, Szentmáry N, Weisensee J, Cayless A, Menapace R, Hoffmann P. Back-calculation of keratometer index based on OCT data and raytracing – a Monte Carlo simulation. *Acta Ophthalmol*. 2021. https://doi.org/10.1111/aos.14794. Epub ahead of print. PMID: 33576147.
13. Levenberg K. A method for the solution of certain problems in least squares. *Quart Appl Math*. 1944;2:164–168.
14. Marquardt D. An algorithm for least-squares estimation of nonlinear parameters. *SIAM J Appl Math*. 1963;11:431–441.
15. Rassow B. Ein Modell für das Gullstrandsche Normalauge [A model of Gullstrand's "normal eye"]. *Ophthalmologica*. 1972;164(2):143–148. https://doi.org/10.1159/000306725

How to cite this article: Langenbucher A, Eppig T, Cayless A, Gatzioufas Z, Wendelstein J, Hoffmann P, et al. Simulation of Corneal imaging properties for near objects. Ophthalmic Physiol Opt. 2021;00:1–9. https://doi.org/10.1111/opo.12861